EVLA Memo #165
The Impact of the New Thermal Gap Receiver Assembly on the Sensitivity of the EVLA at L-band (1–2 GHz)

E. Momjian and R. Perley (NRAO)
and
R. Hayward

November 16, 2012

Abstract

We present sensitivity measurements of the EVLA at L-band between 1 and 2 GHz to assess the impact of the receivers with the new thermal gap assembly. Our on-the-sky test results are consistent with lab measurements, and show that the sensitivity improves by an average value of ∼7% in the frequency range 1–1.55 GHz, and degrades by an average value of ∼3% in the frequency range 1.55–2 GHz. The sensitivity improvement at the lower half of L-band will particularly be valuable for the study of various spectral line transitions that can be observed in this frequency range.

1 Introduction

In early 2012, a new thermal gap assembly was implemented on the L-band receiver system of the EVLA. Lab measurements showed clear improvement in the sensitivity below 1.6 GHz and above 1.95 GHz and a small degradation between 1.6 and 1.95 GHz, in both the RCP and LCP. Figure 1 shows a comparison of the receiver temperature between the old (*red*) and the new (*blue*) thermal gap assemblies of the first L-band receiver that underwent the modification. Upon completion of the lab tests, this receiver was installed on antenna ea05 in March 2012.

To assess the improvement in the sensitivity due to the new thermal gap assembly of the L-band receivers in astronomical observations, we have carried out various on-the-sky tests as soon as antenna ea05 was equipped with the modified receiver. However, the initial observations did not result in any useful data due to severe RFI, both internal and external. Successful observations were finally carried out when the array was in the most extended, A-configuration. At this time, we also had a total of three antennas that were equipped with the new thermal gap assembly L-band receivers.

2 Observations

The EVLA A-configuration observations at L-band were carried out on October 13, 2012, for a total of 0.5 hours. The calibrator source 3C48 (J0137+3309) and a field devoid of strong continuum sources (hereafter "blank field") were observed in this session. The WIDAR correlator was configured to deliver 16 adjacent sub-bands, each with 64 MHz bandwidth, 256 spectral channels, and dual polarization (RR and LL) products. The resulting spectral resolution was 250 kHz. The correlator integration time was set to 1 second.

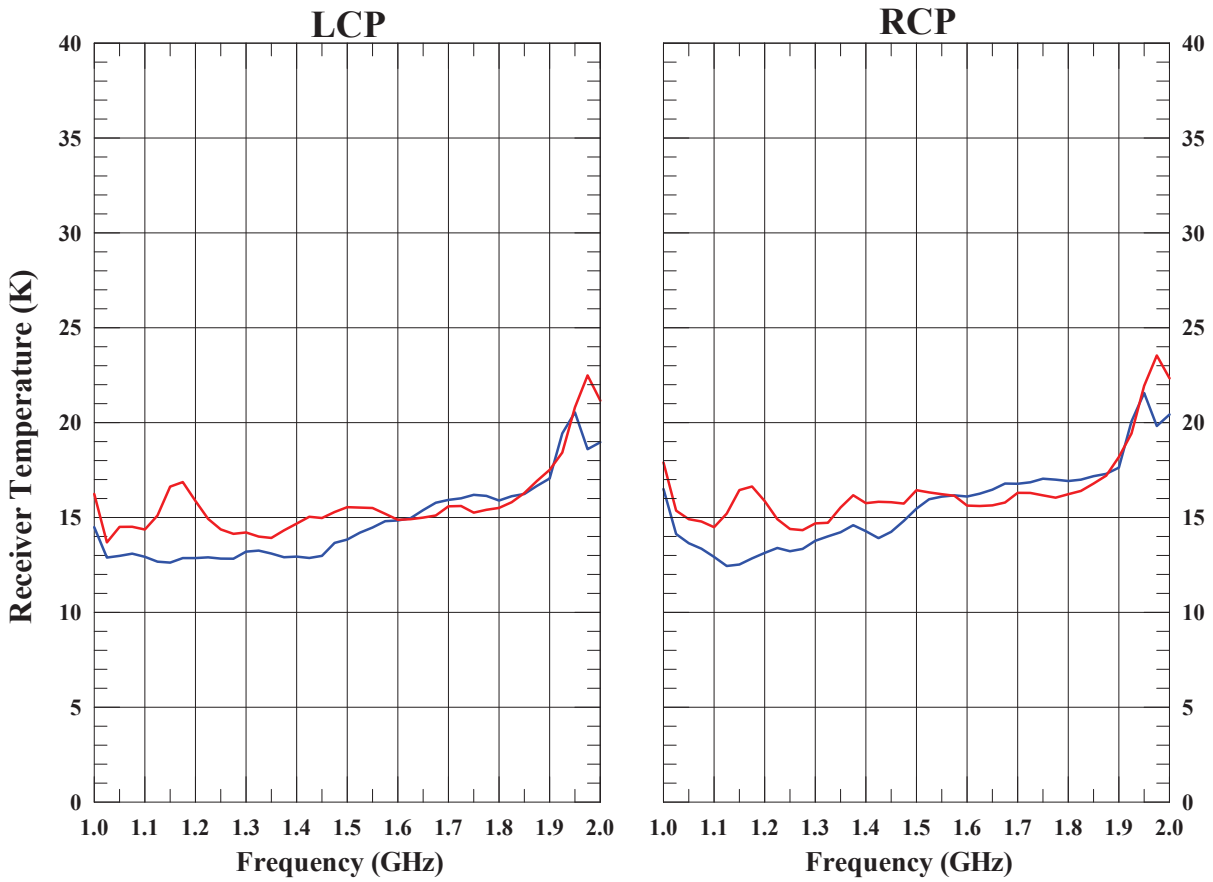

Figure 1: Lab measurements of the receiver temperature of an EVLA L-band receiver with the old (*red*) and new (*blue*) thermal gap assembly. The left-hand side plot is of the LCP, and the right-hand side plot is of the RCP. This receiver was later installed on antenna ea05.

3 Data Reduction and Analysis

Data reduction and analysis were carried out in AIPS. Upon loading the data, antennas that did not have the EVLA-compliant L-band receivers were edited out; see the EVLA Memo #152 (Momjian & Perley 2011) for a detailed discussion on the sensitivity of the EVLA-compliant L-band receivers. The flux density scale was set using the Baars et al. 1977 coefficients for 3C48. After applying a priori flagging and excising integrations affected by interference, antenna based delay, complex gain and bandpass calibration solutions were obtained using the data of the calibrator source 3C48 for each sub-band and polarization product (i.e., RR and LL) separately. These solutions were then applied on the visibilities of the blank field, and spectra were generated to visually inspect its data in order to further ensure the exclusion of spectral channels that were affected by RFI from subsequent analysis.

Using the AIPS task UVHGM, the RMS noise values for Stokes I were measured by fitting Gaussian profiles on the histogram distributions of the blank field's real part of the visibilities. For this, we used channels from each sub-band that were not visibly contaminated by RFI. A 3-channel Hanning-smoothing was applied on the spectra in all the data reduction and analysis steps to reduce the Gibbs ringing phenomenon introduced by strong RFI features at various L-band frequencies.

As noted earlier, only three of the antennas in the data set, namely ea02, ea05, and ea26, were equipped with the L-band receivers that have the new thermal gap assembly. The sensitivity

measurements reported in this memo are based on the average values of the baselines among these three EVLA antennas. For comparison, sensitivity measurements were also obtained using the average values of the baselines among three other antennas with comparable baseline lengths to those noted above.

Multiple background continuum sources in the blank field contribute a total of $S \sim 35$ mJy to our measurements, as determined by imaging one of the sub-bands. A correction was made to account for these background sources as follows:

$$\mathrm{RMS} = \sqrt{(\mathrm{RMS}_h)^2 - (S)^2}, \tag{1}$$

where RMS_h is the noise values obtained through the histogram fittings.

The corrected RMS noise values were then converted to System Equivalent Flux Densities (SEFDs) using the following equation:

$$\mathrm{RMS\ (Jy)} = \frac{1}{2\eta_c\kappa_{hs}} \frac{\mathrm{SEFD\ (Jy)}}{\sqrt{\beta\tau}}, \tag{2}$$

where β is the spectral channel width in Hz and τ is the correlator integration time in seconds. η_c is the WIDAR correlator efficiency, and it is assumed to be 0.93 for the mode used in these observations, and κ_{hs} is the improvement in the signal-to-noise due to the application of the Hanning-smoothing, which is 1.633[1] for a 3-channel Hanning-smoothing.

4 Results and Discussion

Figure 2 shows the SEFD values in the EVLA L-band frequency range $1 - 2$ GHz. The blue curve represents the average SEFD of the baselines among the three antennas that have the L-band receivers with the new thermal gap assembly (ea02, ea05, and ea26). The red curve represents the average SEFD of the baselines among three other antennas that have the old thermal gap assembly and which have comparable baseline lengths to the antennas used in making the measurements reflected by the blue curve. The results show a clear improvement in the sensitivity below 1550 MHz due to the new thermal gap assembly of the L-band receivers, and a slight sensitivity degradation above 1550 MHz.

Figure 3 shows the percentage change in the SEFD due to the new thermal gap assembly relative to the old thermal gap assembly. Positive values reflect lower SEFDs (i.e., improved sensitivity) due to the new thermal gap design. We note that at L-band the receiver temperature is about 50% of the system temperature. Therefore, the percentage improvement in the sensitivity would be about half of the percentage improvement seen in the receiver temperature (Figure 1). This is indeed the case in the on-the-sky test results.

As seen in Figure 3, the sensitivity has improved by an average value of $\sim$7% in the frequency range $1 - 1.55$ GHz. The peak sensitivity improvement is at 1150 MHz and it is by up to $\sim$13%. This is in excellent agreement with the lab measurements (Figure 1) that show a peak in the receiver temperature of the old thermal gap assembly around 1150 MHz. This feature is not seen in the receiver temperature of the new thermal gap assembly, and hence the largest improvement in sensitivity has resulted around this frequency. Above 1.55 GHz, the sensitivity of the receivers with the new thermal gap assembly has degraded by an average value of $\sim$3%, again consistent with the lab measurements shown in Figure 1. We note that our on-the-sky test did not show the sensitivity improvement seen in the lab measurements above 1.95 GHz.

Overall, our results show a net sensitivity improvement that should benefit continuum observations which require the full L-band frequency range. Moreover, the clear sensitivity improvement

[1]The improvement in signal-to-noise due to a 3-channel Hanning-smoothing is $1/\sqrt{0.25^2 + 0.5^2 + 0.25^2}$=1.633

in the lower half of the L-band will be of importance to various spectral line observations such as Galactic and extragalactic HI 21 cm studies (up to redshifts of $z \sim 0.42$ for extragalactic HI), and redshifted OH 18 cm lines ($0.04 \gtrsim z \lesssim 0.72$).

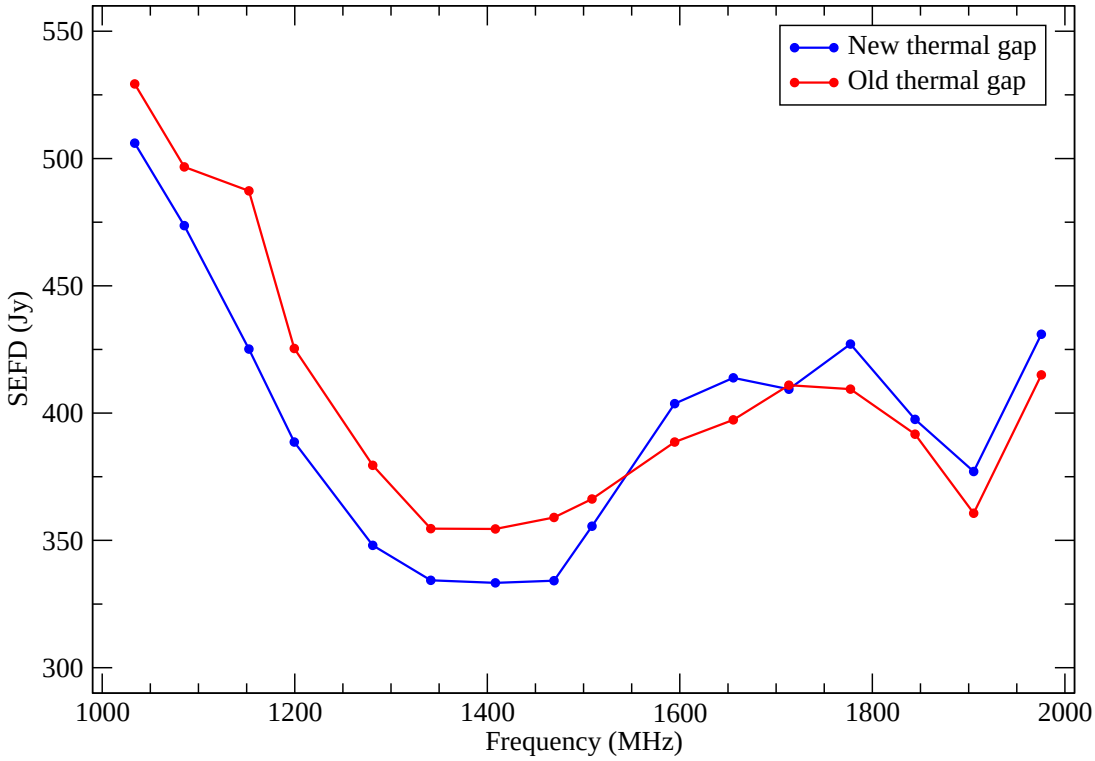

Figure 2: The SEFD values in the EVLA L-band frequency range $1 - 2$ GHz. The blue curve represents the average SEFD of the baselines among the three antennas that have the L-band receivers with the new thermal gap assembly (ea02, ea05, and ea26). The red curve represents the average SEFD of the baselines among three other antennas that have EVLA compliant receivers but with the old thermal gap assembly.

5 Acknowledgements

We would like to thank K. Sowinski and M. Rupen for their help in setting up the test observations.

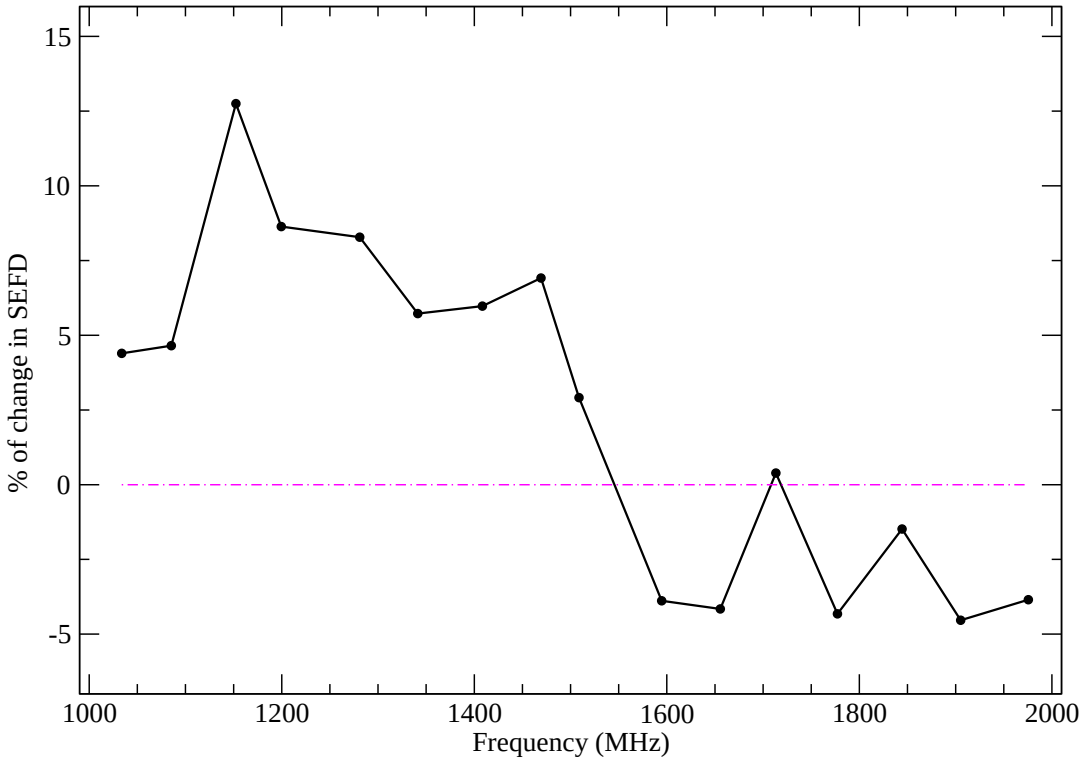

Figure 3: The percentage change in the SEFD due to the new thermal gap assembly relative to the old thermal gap assembly. Positive values reflect lower SEFDs due to the new thermal gap design, and therefore improvement in the sensitivity.